Dopant Distribution in Co-Free High-Energy Layered Cathode Materials

Linqin Mu,[†] Rui Zhang,[‡] Wang Hay Kan,[§,∥] Yan Zhang,[⊥] Luxi Li,[#] Chunguang Kuai,[†] Benjamin Zydlewski,[†] Muhammad Mominur Rahman,[†] Cheng-Jun Sun,[#] Sami Sainio,[⊥] Maxim Avdeev,[∥,¶] Dennis Nordlund,[⊥] Huolin L. Xin,[‡] and Feng Lin*[,†]

[†]Department of Chemistry, Virginia Tech, Blacksburg, Virginia 24061, United States

[‡]Department of Physics and Astronomy, University of California, Irvine, California 92697, United States

[§]Spallation Neutron Source Science Center, Dongguan 523803, China

[∥]Australian Nuclear Science and Technology Organization (ANSTO), New Illawarra Road, Lucas Heights, New South Wales 2234, Australia

[⊥]Stanford Synchrotron Radiation Lightsource, SLAC National Accelerator Laboratory, Menlo Park, California 94025, United States

[#]Advanced Photon Source, Argonne National Laboratory, Argonne, Illinois 60439, United States

[¶]School of Chemistry, The University of Sydney, Sydney, New South Wales 2006, Australia

ABSTRACT: The practical implementation of Co-free, $LiNiO_2$-derived cathodes has been prohibited by their poor cycle life and thermal stability, resulting from the structural instability, phase transformations, reactive surfaces, and chemomechanical breakdown. With the hierarchical distribution of Mg/Ti dual dopants in $LiNiO_2$, we report a Co-free layered oxide that exhibits enhanced bulk and surface stability. Ti shows a gradient distribution and is enriched at the surface, whereas Mg distributes homogeneously throughout the primary particles. The resulting Mg/Ti codoped $LiNiO_2$ delivers a material-level specific energy of ~780 W h/kg at C/10 with 96% retention after 50 cycles. The specific energy reaches ~680 W h/kg at 1C with 77% retention after 300 cycles. Furthermore, the Mg/Ti dual dopants improve the rate capability, thermal stability, and self-discharge resistance of $LiNiO_2$. Our synchrotron X-ray, electron, and electrochemical diagnostics reveal that the Mg/Ti dual dopants mitigate phase transformations, reduce nickel dissolution, and stabilize the cathode−electrolyte interface, thus leading to the favorable battery performance in lithium metal and graphite cells. The present study suggests that engineering the dopant distribution in cathodes may provide an effective path toward lower cost, safer, and higher energy density Co-free lithium batteries.

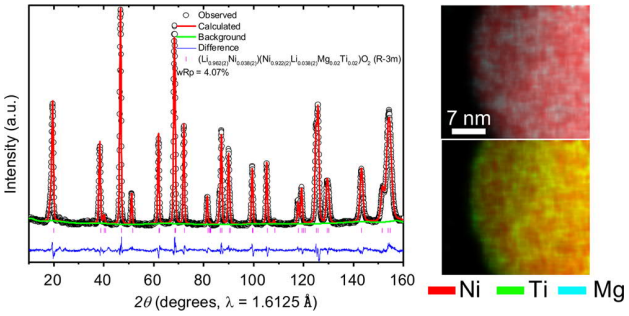

INTRODUCTION

Isostructural to the commercial $LiCoO_2$ in lithium ion batteries, $LiNiO_2$, extensively explored in the 1990s,[1−5] has recently attracted renewed attention in quest of extremely low-Co or completely Co-free layered cathodes to reduce the reliance on high-cost toxic Co resource.[6−11] Owing to the low Ni^{3+}/Ni^{4+} redox potential, $LiNiO_2$ can achieve over 220 mA h/g capacity with a low upper voltage at 4.3 V versus Li^+/Li.[7,8,11] In practice, the available capacity largely varies because of the unfavorable Li off-stoichiometry, that is, Li/Ni cation mixing to form $(Li_xNi_{1-x})_{3a}(Li_{1-y}Ni_y)_{3b}(O_2)_{6c}$[6,12] or Ni-deficient materials.[13,14] Upon charging, $LiNiO_2$ experiences undesired H1 → M → H2 → H3 phase transformations,[2,8,15,16] where H and M represent hexagonal and monoclinic phases, respectively.[4,7,12,17] The 7% volume contraction during the H2 → H3 transformation at 4.15 V versus Li^+/Li triggers severe stress in cathode particles, resulting in crack formation and potentially oxygen release.[2,8] Furthermore, the highly oxidized Ni^{4+} cations in charged particles are thermodynamically unstable, particularly when in contact with the organic electrolyte.[18] The Ni^{4+} ions are readily reduced to a lower oxidation state accompanying the electrolyte decomposition and gas release.[19−22] These challenges, associated with the unstable bulk and surface chemistry, have hindered the implementation of $LiNiO_2$ in practical batteries over the last few decades. The solid solutions of $LiNiO_2$, $LiCoO_2$, and $LiMnO_2$, that is, $LiNi_xMn_yCo_{1-x-y}O_2$ (NMC), have been regarded as an effective strategy to improve the structural and

thermal stability.[20] Indeed, NMC materials have become the pivotal enabler for electric vehicles and consumer electronics. Even though $LiNi_{0.8}Mn_{0.1}Co_{0.1}O_2$ is on the verge of reaching initial market penetration, commercial Li ion batteries based on layered oxide cathodes fail to eliminate Co, a high-cost, toxic, and geographically unevenly distributed element.[23,24] Moreover, the Co mining has been criticized for violating human rights, for instance in the Democratic Republic of the Congo.[25] Therefore, researchers have begun to refocus on the low-Co, high nickel layered oxides, and completely Co-free layered oxides. These practical needs have brought the $LiNiO_2$-based materials back to the spotlight.[6]

There are several potential strategies to address the $LiNiO_2$ challenges,[6] including but not limited to surface coating,[9] bulk doping,[10,26−28] and core−shell hierarchical structures.[29] Among them, the bulk doping with Al^{3+},[30,31] Ti^{4+},[32−34] or Mg^{2+}[35,36] is the most commonly used and the effective method.[6,12] However, a common phenomenon is that the dopants improve the cycle life at the expense of reversible capacity. Nevertheless, these dopants not only break the Li/vacancy ordering thus improving the electrochemical stability but also increase the thermal stability of $LiNiO_2$ cathodes.[6] Several studies have reported that Mg, sitting at the Li^+ site, acts as a structural pillar,[26,27] but Ti, sitting at the Ni^{3+} site, destabilizes the Li/vacancy ordering.[6] To date, most studies have assumed the homogeneous distribution of dopants in battery particles.[30] Furthermore, the doping studies with inert elements for $LiNiO_2$ have predominantly focused on a single dopant.[37] Multielement doping for the layered oxide materials has been attempted in some studies,[38−40] but the doping mechanism remains unclear and debatable. When introducing more than one dopant, it is still obscure how dopants may redistribute inside the particles or exhibit different functionalities in battery performance. Thus, we believe that there is a large space to optimize the distribution of dual dopants to simultaneously improve the bulk and surface chemistry of $LiNiO_2$-based cathodes.

Herein, we design and synthesize a new Co-free cathode material, low-concentration Mg/Ti dual-doped $LiNiO_2$, in which Mg distributes homogenously in battery particles and Ti is mainly enriched at the top surface (i.e., hierarchical distribution of Mg/Ti dual dopants). Synchrotron X-ray and neutron scattering diagnostics reveal that both dopants occupy the Ni sites in the $LiNiO_2$ lattice. The hierarchical distribution of Mg/Ti dual dopants not only destabilizes the Li/vacancy ordering thus leading to smooth voltage profiles but also stabilizes the surface oxygen thus mitigating the Ni dissolution.[41] As a result, compared to the baseline $LiNiO_2$ material, the new Co-free cathode material allows for enhanced specific energy, cycle life, rate capability, self-discharge resistance, and thermal stability. These results lay the foundation for manipulating the doping chemistry and dopant spatial distribution in Co-free layered oxides for safer and higher energy lithium batteries.

■ RESULTS AND DISCUSSION

The baseline $LiNiO_2$ (LNO) and Mg/Ti dual-doped $LiNiO_2$ (Mg/Ti−LNO) were synthesized by a coprecipitation method (see Experimental Methods). The pure layered phase (space group: $R\bar{3}m$) was verified by synchrotron X-ray diffraction (XRD) (Figure S1) and scanning transmission electron microscopy (STEM) (Figure 1c,d). The polycrystalline secondary particles consist of 50−200 nm primary particles

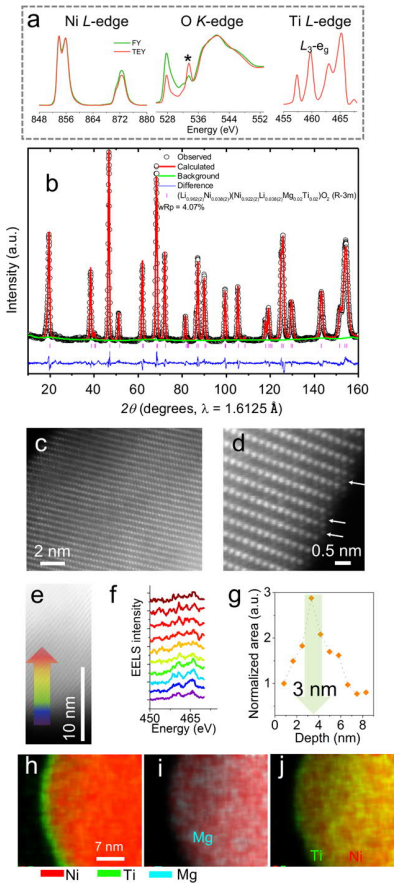

Figure 1. Characterizations of the pristine Mg/Ti−LNO material. (a) Ni/Ti L-edge and O K-edge soft XAS spectra, the * represents carbonate species; (b) ND and Rietveld refinement; (c,d) annular dark-field STEM images of the primary particle; (e) EELS spectra scanning pathway from the surface to the subsurface with the increment of 0.8 nm for each spectrum; (f) Ti L-edge EELS spectra recorded with the scanning pathway (from the bottom purple to the top dark red spectra); (g) normalized peak area of Ti L-edge EELS as a function of the scanning depth; and (h) STEM−EDS mapping of the Ni (red) and Ti (green) in the composition scale and (i,j) concentration scale on the selected particle.

(Figure S2). The Brunauer−Emmett−Teller specific surface areas of LNO and Mg/Ti−LNO were 1.1 and 0.3 m^2/g, respectively. This suggests that the dual dopants facilitated the formation of much denser secondary particles, which might mitigate side reactions with the electrolyte. In Ni-rich layered oxides, the Li/Ni cation mixing (antisite defect) is inevitable, leading to the formation of off-stoichiometric materials.[42] This usually results in Li-deficient phases with slightly reduced Ni cations (Ni oxidation state $<Ni^{3+}$).[19] Indeed, the soft X-ray absorption spectroscopy (XAS) revealed that the Ni oxidation state was slightly lower than Ni^{3+} (Figure 1a). Additionally, we found that the Ti^{4+} dopant was fully accommodated in the layered lattice with no TiO_2 phase, as indicated by the absence of the Ti L_3-e_g splitting (Figure 1a).[43] The presence of carbonate species was evident at the surface (Figure 1a).[22,44,45] For the $LiNiO_2$ material, the Ni at the surface was slightly reduced and the carbonate species was also present on the surface (Figure S3). Furthermore, we performed neutron diffraction (ND) and Rietveld refinement to determine that ∼4% Ni occupied the Li sites (Figure 1b). The Rietveld

refinement also suggested that both Mg^{2+} and Ti^{4+} occupied the Ni sites without the presence of impurity phases. The structural parameters are presented in Table S1. The cation-mixing was unidentifiable in the atomic-resolution annular dark-field STEM (ADF-STEM) image of the bulk because of the small amount (Figure 1c). Yet, a thin layer of Ni sitting at the Li sites was observed at the surface (Figure 1d). These results suggested that the cation mixing might prefer lodging at the surface. To further probe the Ti distribution, we performed electron energy loss spectroscopy (EELS) scanning from the particle surface to the subsurface (Figure 1e,f). The Ti^{4+} L-edge signal was mainly detected in the first five spectra, and the normalized Ti^{4+} L-edge intensity confirmed that the Ti^{4+} dopant was enriched at the top few nanometers of the particles (Figure 1f,g). The energy dispersive X-ray spectroscopy (EDS) mapping results (Figure 1h–j) revealed that Mg^{2+} was evenly distributed, whereas Ti^{4+} was enriched at the top ~3 nm, which was consistent with the EELS mapping. The slow Ti^{4+} diffusion kinetics during calcination and its low solid solubility in $LiNiO_2$ might be the origins of forming the unique hierarchical distribution. The surface-enriched Ti can form strong ionic bonding with the oxygen anion, thus reducing the TM 3d–O 2p hybridization and inhibiting the surface oxygen loss.[38,46–48] The bulk Mg doping may stabilize the bulk crystal structure and mitigate the undesired phase transformations.[26] Collectively, such a hierarchical distribution of dopants may simultaneously offer surface and bulk stability thus delivering favorable electrochemical properties.

We evaluated the battery performance of the Mg/Ti–LNO cathode in half and full cells at 2.5–4.4 V versus Li^+/Li at 22 °C. Such a high upper cutoff voltage allowed us to investigate the advantages of the dual dopants in limiting phase transformations and mitigate the cathode–electrolyte interfacial reactions under aggressive conditions.[8] Compared with LNO, the Mg/Ti–LNO showed much smoother charge/discharge profiles (Figure 2a, in particular within the 4.0–4.4 and 3.7–3.5 V ranges), indicating that phase transformations and Li/vacancy ordering are suppressed.[9,32,37] The galvanostatic intermittent titration (GITT) measurements showed that the open circuit voltages (OCVs) upon discharging were close in these materials, but the Mg/Ti–LNO cathode had a higher charging OCV (Figure S4), suggesting that the dual dopants slightly enlarged the polarization during the initial cycles.[37] At C/10, the Mg/Ti–LNO cathode delivered a 208 mA h/g discharge capacity which was slightly lower than the baseline LNO (225 mA h/g, Figure S5). However, the charge/discharge profiles (Figure 2b) of Mg/Ti–LNO after 50 cycles overlapped well with the second cycle (i.e., minimal increase of cell polarization), delivering a 95% capacity retention that was remarkably higher than the baseline LNO (73.6%, Figures 2a and S5). We plotted dQ/dV versus voltage based on the charge/discharge profiles of the two cathodes (Figure 2c). Consistent with the charge/discharge profiles, the Mg/Ti–LNO displayed smoother and fewer peaks than the LNO (Figure 2c).[5] After 50 cycles, we observed negligible changes (neither the intensity nor the peak position) in the dQ/dV versus voltage curve of the Mg/Ti–LNO (Figure 2c). However, the rapid fading at around 3.6 and 4.1 V was observed in the LNO, which was associated with the H1 → M and H2 → H3 phase transformations, respectively.[7] The cyclic voltammetry (CV) results for these cathodes were consistent with the dQ/dV evolution (Figure S6). In addition, the rate capability of the Mg/Ti–LNO cathode was better than that of

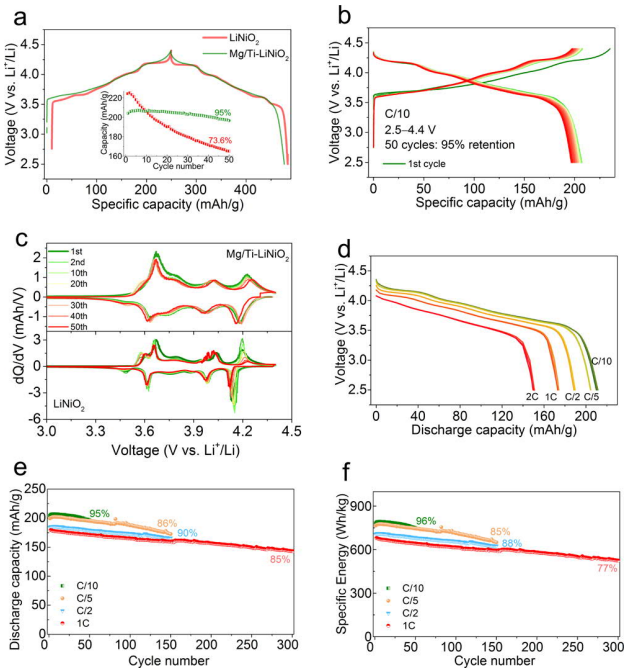

Figure 2. Electrochemical performance of the half cells containing the Mg/Ti–LNO cathode at 22 °C within 2.5–4.4 V. (a) Voltage profiles of the LNO and Mg/Ti–LNO at C/10 (20 mA/g), the insert shows the discharge capacity as a function of the cycle number; (b) voltage profiles in the first 50 cycles at C/10; (c) dQ/dV curves of the two cathodes derived from the voltage profiles at C/10; (d) discharge voltage profiles at the symmetrical constant currents of C/10, C/5, C/2, 1C and 2C; (e) long-term cycling performance; and (f) specific energy retention at different C-rates.

the LNO (the 2C capacity maintained 76% of the C/10 capacity in the Mg/Ti–LNO cathode) (Figures 2d and S7). At C/5, C/2 and 1C (Figure 2e), the initial discharge capacity was 200, 180, and 175 mA h/g, respectively. The capacity retention after 150 cycles at C/5 and C/2 was 86 and 90%, respectively. Furthermore, 85% capacity retention was achieved at 1C for 300 cycles. The material-level specific energy was ~780 W h/kg at C/10 and C/5, and ~680 W h/kg at C/2 and 1C (Figure 2f), which were higher than many reported Ni-rich NMC cathodes.[28,49,50] The energy retention was 96, 85, 88, and 77% at C/10, C/5, C/2, and 1C after their corresponding numbers of cycles, as shown in Figure 2f. The performance at elevated temperatures is also an important metric for practical batteries. The cells containing the LNO and Mg/Ti–LNO cathodes were tested at 60 °C. The capacity retentions at C/3 were 66 and 78% after 50 cycles for the LNO and Mg/Ti–LNO cathodes, respectively (Figure S8). The electrochemical performance of Co-free Mg/Ti–LNO surpassed many reported $LiNiO_2$-based materials, as summarized in Table S2. Finally, we assembled full cells using graphite as the anode (Figure S9). The full cells (Figure S10) delivered a 200 mA h/g discharge capacity at C/2 with an 82% capacity retention after 100 cycles at 22 °C.

The dual dopants also enhanced the surface stability, minimized the Ni dissolution, improved the thermal stability,[51] and increased the self-discharge resistance of the Co-free $LiNiO_2$-based material. The transition metal dissolution (nickel in this case), representing one aspect of the surface stability, is a challenge for Ni-rich NMC materials.[52,53]

Synchrotron X-ray fluorescence microscopy (XFM), a highly sensitive technique for quantitative (sub ppm) and spatially resolved analysis of trace elements, was performed on the lithium anode after 50 cycles at C/3 (Figures 3a,b, S11).

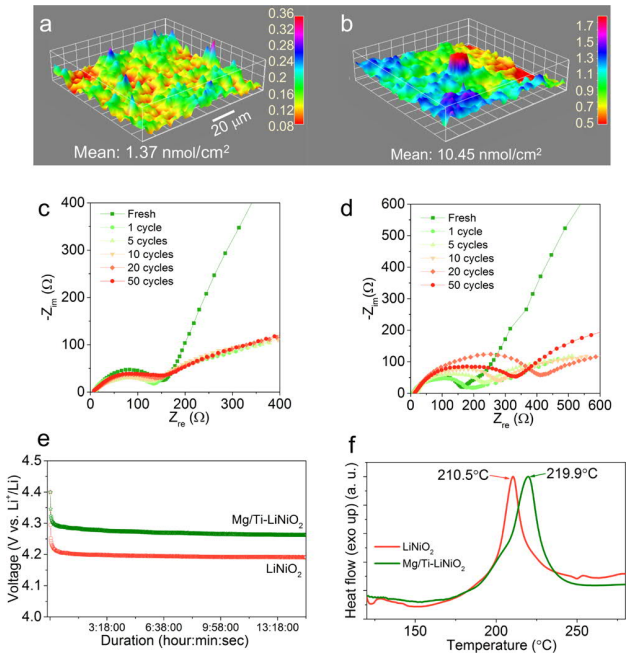

Figure 3. XFM (the colors represent Ni concentration) on the lithium metals countered with (a) Mg/Ti−LNO and (b) LNO cathodes operated at C/3 after 50 cycles within 2.5−4.4 V at 22 °C; Nyquist plots of the half cells containing the (c) Mg/Ti−LNO and (d) LNO cathodes at the fresh state, 1 cycle, 5 cycles, 10 cycles, 20 cycles, and 50 cycles at the discharged states. (e) Voltage evolutions of the two cells charged to 4.4 V and rested for 14 h; (f) DSC analysis of the two wet cathodes (with electrolyte) at 4.4 V charged state with a scan rate of 10°/min.

Overall, the lithium anode collected from the Mg/Ti−LNO cell showed nearly 10 times lower Ni concentration than that collected from the LNO cell. In addition, the Ni distribution was also more uniform in the former sample. We further measured the electrochemical impedance spectroscopy of the cells at various states (Figure 3c,d). The interfacial resistance (high frequency, semicircle on the left) was ∼150 Ω in both cells in the pristine state. For the Mg/Ti−LNO cell, the resistance remained relatively stable during cycling (Table S3). However, the resistance gradually increased up to 20 cycles and decreased slightly after 50 cycles in the LNO cell (Table S3). The similar phenomenon (Table S3) was also observed for the resistance originated from the charge transfer process (low frequency, semicircle on the right). These results indicated that the Mg/Ti dual dopants improved the stability of the cathode−electrolyte interface, which might be one of the factors responsible for the improved cycling performance.[9,40] The self-discharge resistance and thermal stability were also improved with the Mg/Ti dual dopants. The cells were charged to 4.4 V and rested for 14 h to reach the equilibrium state (Figure 3e). During the initial resting, the voltage decreased dramatically to 4.3 and 4.2 V for the Mg/Ti−LNO and LNO cathodes, respectively. Overall, the Mg/Ti−LNO exhibited stronger self-discharge resistance. The exothermic peak in the differential scanning calorimetry (DSC) analysis represents the thermal stability of a cathode in the charged state (in this case, charged to 4.4 V). The Mg/Ti−LNO cathode showed higher thermal stability with an exothermic temperature of 219.9 °C as opposed to 210 °C in the LNO cathode (Figure 3f).[26,37,46,54]

The charge compensation mechanism, local and global structural stabilities of the Mg/Ti−LNO cathode were studied using a suite of advanced synchrotron X-ray and electron diagnostics, including synchrotron XRD, hard and soft XAS, extended X-ray absorption fine structure (EXAFS) and the associated wavelet transform analysis, and electron microscopy. Upon charging, the Ni K-edge shifted to higher energy, indicating the oxidization of Ni^{3+} to partially Ni^{4+} (Figure 4a).

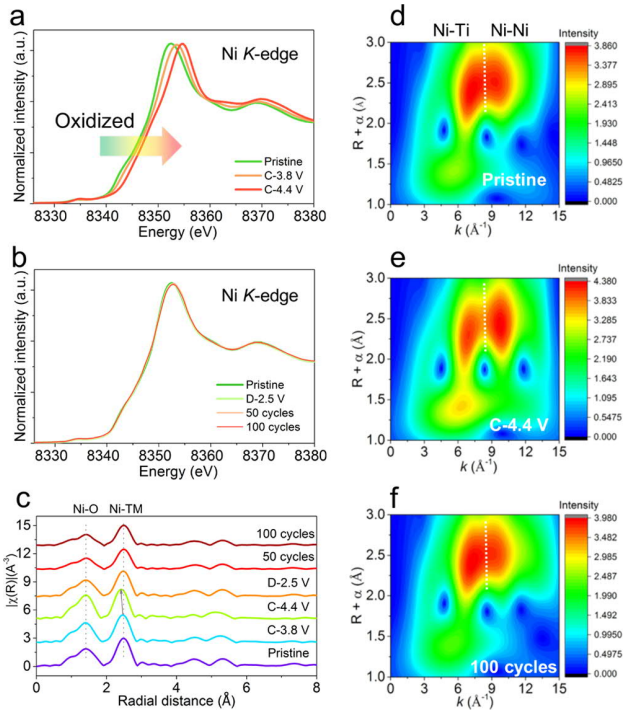

Figure 4. Charge compensation mechanism and Ni local environment evolution. Ex situ Ni K-edge XANES of the Mg/Ti−LNO cathode upon (a) charging and (b) discharging and after long cycling; (c) ex situ Ni K-edge EXAFS of the Mg/Ti−LNO cathode at various states; wavelet transforms for the K3-weighted Ni K-edge EXAFS of the Mg/Ti−LNO cathode at the (d) pristine state, (e) charged to 4.4 V, and (f) discharged to 2.5 V after 100 cycles.

Upon discharging (Figure 4b), the edge shifted back to the original state. After 50 and 100 cycles, there was negligible change of the Ni oxidation state, indicating the good bulk reversibility of the Ni^{3+}/Ni^{4+} redox couple. The EXAFS analysis showed two Ni local environments, that is, Ni−O at 1.7 Å and Ni−TM at 2.5 Å (Figure 4c). Upon charging, the Ni−TM distance reduced slightly, while the Ni−O bonding underwent negligible change because of the Jahn−Taller distorsion.[17] In the discharged state after 1, 50, and 100 cycles, the Ni−O and Ni−TM distances did not change, implying the bulk structural stability of the local environment. We further performed the EXAFS wavelet transform analysis, a powerful method for distinguishing the backscattering atoms to analyze the Ni local environment (Figure 4d−f).[55] In the pristine state (Figure 4d), we observed that the bonding at 2.5 Å ("$R + \alpha$") split into two in the k space, which were associated with the Ni−Ni (right)

and Ni–Ti (left).[55] The wavelet transform analysis further supported our conclusion that the Ti dopant occupies the Ni site in the $R\bar{3}m$ lattice. The splitting became wider in the charged state (4.4 V) (Figure 4e) and recovered to the original state after 100 cycles (Figure 4f), demonstrating the stability and reversibility of the local coordination environment. Meanwhile, we also conducted XRD to elucidate the global structural stability (Figure S12). Upon charging, the (003) peak shifted to the lower angle, while the (104) peak moved to the higher angle, suggesting the expansion of the *c*-axis and the contraction of the *a*-*b* plane. Upon discharging, these peaks went through the opposite shifting and recovered to its original state. After 100 cycles at C/3, the layered structure maintained well in spite of the slight off-set of the (003) peak. The peak shift was associated with the minor capacity loss because of the Li loss from the lattice. Indeed, the soft XAS results illustrated that the surface Li loss was accompanied by the surface Ni reduction after long cycles (Figure S13).[18,21,22] In summary, the results indicate that although the Mg/Ti dual dopants did not completely eliminate the surface degradation, they significantly enhanced local structural stability, alleviated the Ni dissolution, and improved the thermal stability of the LNO material.

Because Li ion diffusion coefficient is a key factor to influence the rate capability of an electrode material, we also investigated the kinetic performance of the Co-free cathode by GITT (Figure 5a).[56,57] The hysteresis (between the charging

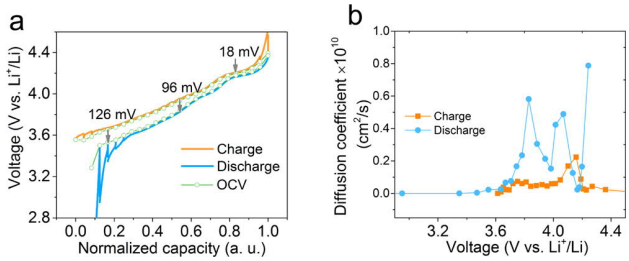

Figure 5. Kinetics performance of the half cells containing the Mg/Ti–LNO cathode. (a) GITT curves at the second cycle and its derived OCV curve of the cell upon charging/discharging at C/20 for 1 h and following with 10 h rest and (b) the apparent chemical diffusion coefficient as a function of voltage derived from the GITT curves.

OCV and discharging OCV) decreased as the voltage increased (i.e., increased degree of delithiation), indicating that the reaction kinetics got improved as more lithium vacancies were created during charging. Specifically, the polarization at 3.6 V was 126 mV, which was larger than those at 4.0 and 4.2 V. The equation $\tilde{D} = \frac{4}{\pi\tau}\left(\frac{m_B V_M}{M_B S}\right)^2\left(\frac{\Delta E_S}{\Delta E_\tau}\right)^2$ (see details in SI) was used to calculate the apparent Li^+ diffusion coefficient at various states of charge (Figure 5b). In general, the discharging kinetics was better than the charging kinetics. The D_{Li^+} was in the order of 10^{-10} to 10^{-11} cm^2/s, which is comparable to other reported Ni-rich NMC materials.[58,59] The Li^+ diffusion within 4.3–3.7 V during discharging was better than other states, except two sudden drops at 4.0 and 4.2 V. These two drops were likely associated with the inhibited M → H2 and H2 → H3 phase transformations, respectively.[5] We also used cyclic voltammogram at various scan rates (see details in the SI) to estimate the D_{Li^+} in the LNO and Mg/Ti–LNO materials (Figures S14 and S15). We obtained Li^+ diffusion coefficient in the order of 10^{-11} and 10^{-10} cm^2/s for LNO and Mg/Ti–LNO materials, respectively (Figures S14 and 15). The results suggest that the Mg/Ti dual dopants slightly facilitated Li^+ kinetics.

CONCLUSIONS

To make batteries and electric vehicles more sustainable and environment-friendly, efforts must be made to significantly reduce or even completely eliminate Co. In this study, we expanded the conventional doping strategy and proposed the concept of manipulating the dopant distribution in battery particles to simultaneously enhance the surface and bulk stability of Co-free, $LiNiO_2$-based cathodes. We developed hierarchical distribution of Mg/Ti dual dopants in Co-free layered oxides as the initial platform to investigate the concept. The advanced spectroscopic and imaging diagnostics reveal that Ti showed a gradient distribution and was enriched at the surface, whereas Mg distributes homogeneously throughout the particles. Both dopants were well accommodated in the Ni sites of the layered structure. The dual dopants in the bulk reduced the Li/vacancy ordering, smoothened voltage profiles, and suppressed irreversible phase transformations. The interfacial stability of the Mg/Ti–LNO material was improved,[41] leading to mitigated Ni dissolution, reduced cell impedance, improved thermal stability, and better self-discharge resistance. This new Co-free layered cathode achieved a specific discharge capacity of 208 mA h/g at C/10 and 95% capacity retention after 50 cycles at C/10 within 2.5–4.4 V. The capacity retention was 85% at 1C after 300 cycles. The material-level specific energy was ~780 W h/kg at C/10 and ~680 W h/kg at 1C. While there were no extensive studies attempting to engineer the dopant distribution in battery materials, our promising battery performance suggests that there is a large space to manipulate the three-dimensional distribution of dopants to improve the stability of $LiNiO_2$. Such a concept can be readily extended to other material systems, including Li ion and Na ion chemistries. We recommend that further studies of this new material should focus optimizing the cathode–electrolyte interplay, which entails more efforts in developing new electrolyte systems.

EXPERIMENTAL METHODS

Material Synthesis. The baseline $LiNiO_2$ and Mg/Ti–$LiNiO_2$ were synthesized by a coprecipitation method followed by high temperature calcination. The transition-metal solution (0.1 mol $NiSO_4{\cdot}6H_2O$ dissolved in 100 mL of aqueous solution), starting solution (40 mL of NaOH and $NH_3{\cdot}H_2O$ aqueous solution with a molar ratio $NaOH/NH_3$ = 1.2, pH value was adjusted to 11.0), and base solution (100 mL of NaOH and $NH_3{\cdot}H_2O$ aqueous solution with a molar ratio $NaOH/NH_3$ = 1.2) were made and separately stored under N_2 protection. The transition-metal solution and base solution were simultaneously pumped into the starting solution at a feed rate of ~2 mL/min with continuous stirring at 55 °C under N_2 protection. The feed rate of the base solution was frequently tuned to keep the pH at 11.0 ± 0.2. The precipitate was collected, washed, and filtered with deionized water and dried in a vacuum oven overnight at 105 °C. The dried precursor was then mixed with LiOH thoroughly and calcined under air flow (2 L/min) at 460 °C for 2 h and then at 675 °C for 6 h to obtain the final $LiNiO_2$ powder. For the Mg/Ti–$LiNiO_2$, the transition-metal solution (0.096 M $NiSO_4{\cdot}6H_2O$, 0.002 M $MgSO_4{\cdot}7H_2O$, and 0.002 M $TiOSO_4$ dissolved in 100 mL of aqueous solution), starting solution (40 mL of NaOH and $NH_3{\cdot}H_2O$ aqueous solution with a molar ratio $NaOH/NH_3$ = 1.2, pH value was adjusted to 11.0), and base solution (100 mL of NaOH and $NH_3{\cdot}$

H_2O aqueous solution with a molar ratio $NaOH/NH_3$ = 1.2) were made and separately stored under N_2 protection. The transition metal solution and base solution were simultaneously pumped into the starting solution at a feed rate of ~2 mL/min with continuous stirring at 55 °C under N_2 protection. The feed rate of the base solution was frequently tuned to keep the pH at 11.0 ± 0.2. The precipitate was collected, washed, and filtered with deionized water and dried in vacuum oven overnight at 105 °C. The dried precursor was then mixed with LiOH thoroughly and calcined under air flow (2 L/min) at 460 °C for 2 h and then at 700 °C for 6 h to obtain the final Mg/Ti−$LiNiO_2$ powder.

Electrochemical Characterization. The Co-free cathode powders were processed into the electrode immediately following the high temperature calcination, and the acetylene carbon and poly(vinylidene difluoride) (PVdF) were stored in a humidity-controlled dry box prior to the electrode preparation. The composite cathodes were prepared by spreading the slurry (*N*-methyl-2-pyrrolidone as the solvent) with active materials (90 wt %), acetylene carbon (5 wt %), and PVdF (5 wt %) as the binder, and casting them on carbon-coated aluminum foils. The graphite anode was prepared by spreading the slurry (*N*-methyl-2-pyrrolidone as the solvent) with active materials (90 wt %), acetylene carbon (5 wt %), and PVdF (5 wt %) as the binder and casting them on copper foils. The cathode and graphite electrodes were punched into disks of a diameter of 10 mm. The disks were then dried overnight at 120 °C in a vacuum oven and transferred into an Ar-filled glove box. The cathode active mass loading was ~1.4 mA h/cm^2 (7 mg/cm^2) and the graphite mass loading of ~5.2 mg/cm^2. CR2032 coin cells were assembled in a Ar-filled glovebox using the composite cathode, lithium foil as the anode, Whatman glass fiber (1827-047934-AH) as the separator, and 1 M $LiPF_6$ dissolved in ethylene carbonate (EC) and ethyl methyl carbonate with 2 wt % vinylene carbonate as the electrolyte. All cells were cycled with an electrochemical workstation (Wuhan Land Company) at 22 and 60 °C in an environmental chamber. The specific energy was calculated using the LANDdt software. 1C was defined as fully charging a cathode in 1 h, corresponding to a specific current density of 200 mA/g.

The details of material characterization and diffusion coefficient analysis can be found in the Supporting Information.

AUTHOR INFORMATION

Corresponding Author

*E-mail: fenglin@vt.edu.

ORCID

Linqin Mu: 0000-0003-4421-4820
Wang Hay Kan: 0000-0002-1663-2999
Muhammad Mominur Rahman: 0000-0001-6814-456X
Sami Sainio: 0000-0002-9268-0124
Maxim Avdeev: 0000-0003-2366-5809
Feng Lin: 0000-0002-3729-3148

Author Contributions

F.L. conceived and led the project. L.M. and F.L. designed the experiments. L.M. performed the synthesis, SEM, synchrotron, and electrochemical measurements. C.K. and B.Z. assisted the synthesis. W.H.K. and M.A. performed the ND and refinement. Y.Z., S.S,. and D.N. performed the soft XAS measurements. C.-J.S. collected the hard XAS data. M.M.R. participated in the synchrotron experiments. R.Z. and H.L.X. conducted the TEM characterization. F.L. and L.M. analyzed the data and wrote the manuscript with the help of all the coauthors.

Notes

The authors declare no competing financial interest.

ACKNOWLEDGMENTS

This material is based upon the work supported by the U.S. Department of Energy's Office of Energy Efficiency and Renewable Energy (EERE) under the award number: DE-EE0008444. W.H.K. appreciates the beamtime in ECHIDNA granted from Australian Centre for Neutron Scattering (CSNS) in ANSTO. The use of the Stanford Synchrotron Radiation Lightsource, SLAC National Accelerator Laboratory, is supported by the U.S. Department of Energy, Office of Science, Office of Basic Energy Sciences under Contract No. DE-AC02-76SF00515. Professor Greg Liu and Dr. Tianyu Liu are acknowledged for collecting the N_2 physisorption data. This research used resources of the Advanced Photon Source, a U.S. Department of Energy (DOE) Office of Science User Facility operated for the DOE Office of Science by Argonne National Laboratory under contract no. DE-AC02-06CH11357. W.H.K. thank the support from the National Natural Science Foundation of China (11805034 and 21704105). This report was prepared as an account of work sponsored by an agency of the United States Government. Neither the United States Government nor any agency thereof, nor any of their employees, makes any warranty, express or implied, or assumes any legal liability or responsibility for the accuracy, completeness, or usefulness of any information, apparatus, product, or process disclosed, or represents that its use would not infringe privately owned rights. Reference herein to any specific commercial product, process, or service by trade name, trademark, manufacturer, or otherwise does not necessarily constitute or imply its endorsement, recommendation, or favoring by the United States Government or any agency thereof. The views and opinions of authors expressed herein do not necessarily state or reflect those of the United States Government or any agency thereof.

REFERENCES

(1) Ohzuku, T.; Ueda, A.; Nagayama, M.; Iwakoshi, Y.; Komori, H. Comparative study of $LiCoO_2$, $LiNi_{12}Co_{12}O_2$ and $LiNiO_2$ for 4 volt secondary lithium cells. *Electrochim. Acta* **1993**, *38*, 1159−1167.

(2) Ohzuku, T.; Ueda, A.; Nagayama, M. Electrochemistry and Structural Chemistry of $LiNiO_2$ ($R\bar{3}m$) for 4 Volt Secondary Lithium Cells. *J. Electrochem. Soc.* **1993**, *140*, 1862−1870.

(3) Dahn, J. R.; von Sacken, U.; Juzkow, M. W.; Al-Janaby, H. Rechargeable $LiNiO_2$/Carbon Cells. *J. Electrochem. Soc.* **1991**, *138*, 2207−2211.

(4) Arai, H.; Okada, S.; Sakurai, Y.; Yamaki, J.-i. Reversibility of $LiNiO_2$ cathode. *Solid State Ionics* **1997**, *95*, 275−282.

(5) Barker, J.; Koksbang, R.; Saidi, M. Y. An electrochemical investigation into the lithium insertion properties of Li_xNiO_2 ($0 \leq x \leq 1$). *Solid State Ionics* **1996**, *89*, 25−35.

(6) Bianchini, M.; Roca-Ayats, M.; Hartmann, P.; Brezesinski, T.; Janek, J. There and Back Again-The Journey of $LiNiO_2$ as a Cathode Active Material. *Angew. Chem., Int. Ed.* **2019**, *58*, 10434−10458.
(7) Li, H.; Zhang, N.; Li, J.; Dahn, J. R. Updating the Structure and Electrochemistry of Li_xNiO_2 for $0 \leq x \leq 1$. *J. Electrochem. Soc.* **2018**, *165*, A2985−A2993.
(8) Yoon, C. S.; Jun, D.-W.; Myung, S.-T.; Sun, Y.-K. Structural Stability of $LiNiO_2$ Cycled above 4.2 V. *ACS Energy Lett.* **2017**, *2*, 1150−1155.
(9) Yoon, C. S.; Kim, U.-H.; Park, G.-T.; Kim, S. J.; Kim, K.-H.; Kim, J.; Sun, Y.-K. Self-Passivation of a $LiNiO_2$ Cathode for a Lithium-Ion Battery through Zr Doping. *ACS Energy Lett.* **2018**, *3*, 1634−1639.
(10) Yoon, C. S.; Choi, M.-J.; Jun, D.-W.; Zhang, Q.; Kaghazchi, P.; Kim, K.-H.; Sun, Y.-K. Cation Ordering of Zr-Doped $LiNiO_2$ Cathode for Lithium-Ion Batteries. *Chem. Mater.* **2018**, *30*, 1808−1814.
(11) Markevich, E.; Salitra, G.; Talyosef, Y.; Kim, U.-H.; Ryu, H.-H.; Sun, Y.-K.; Aurbach, D. High-Performance $LiNiO_2$ Cathodes with Practical Loading Cycled with Li metal Anodes in Fluoroethylene Carbonate-Based Electrolyte Solution. *ACS Appl. Energy Mater.* **2018**, *1*, 2600−2607.
(12) Delmas, C.; Croguennec, L. Layered $Li(Ni, M)O_2$ Systems as the Cathode Material in Lithium-Ion Batteries. *MRS Bull.* **2011**, *27*, 608−612.
(13) Tabuchi, M.; Kuriyama, N.; Takamori, K.; Imanari, Y.; Nakane, K. Appearance of Lithium-Excess $LiNiO_2$ with High Cyclability Synthesized by Thermal Decomposition Route from $LiNiO_2$-Li_2NiO_3 Solid Solution. *J. Electrochem. Soc.* **2016**, *163*, A2312−A2317.
(14) Kobayashi, Y.; Tabuchi, M.; Miyashiro, H.; Kuriyama, N. A new design of highly reversible $LiNiO_2$: Defect formation in transition metal site. *J. Power Sources* **2017**, *364*, 156−162.
(15) de Biasi, L.; Schiele, A.; Roca-Ayats, M.; Garcia, G.; Brezesinski, T.; Hartmann, P.; Janek, J. Phase Transformation Behavior and Stability of $LiNiO_2$ Cathode Material for Li-Ion Batteries Obtained from In Situ Gas Analysis and Operando X-Ray Diffraction. *ChemSusChem* **2019**, *12*, 2240−2250.
(16) Li, H.; Liu, A.; Zhang, N.; Wang, Y.; Yin, S.; Wu, H.; Dahn, J. R. An Unavoidable Challenge for Ni-rich Positive Electrode Materials for Lithium-Ion Batteries. *Chem. Mater.* **2019**, *31*, 7574−7583.
(17) Croguennec, L.; Pouillerie, C.; Mansour, A. N.; Delmas, C. Structural characterisation of the highly deintercalated LixNi1.02O2 phases (with $x \leq 0.30$). *J. Mater. Chem.* **2001**, *11*, 131−141.
(18) Lin, F.; Nordlund, D.; Markus, I. M.; Weng, T.-C.; Xin, H. L.; Doeff, M. M. Profiling the nanoscale gradient in stoichiometric layered cathode particles for lithium-ion batteries. *Energy Environ. Sci.* **2014**, *7*, 3077−3085.
(19) Xu, J.; Hu, E.; Nordlund, D.; Mehta, A.; Ehrlich, S. N.; Yang, X.-Q.; Tong, W. Understanding the Degradation Mechanism of Lithium Nickel Oxide Cathodes for Li-Ion Batteries. *ACS Appl. Mater. Interfaces* **2016**, *8*, 31677−31683.
(20) Schipper, F.; Erickson, E. M.; Erk, C.; Shin, J.-Y.; Chesneau, F. F.; Aurbach, D. Review—Recent Advances and Remaining Challenges for Lithium Ion Battery Cathodes: I. Nickel-Rich, $LiNi_xCo_yMn_zO_2$. *J. Electrochem. Soc.* **2017**, *164*, A6220−A6228.
(21) Lin, F.; Markus, I. M.; Nordlund, D.; Weng, T.-C.; Asta, M. D.; Xin, H. L.; Doeff, M. M. Surface reconstruction and chemical evolution of stoichiometric layered cathode materials for lithium-ion batteries. *Nat. Commun.* **2014**, *5*, 3529.
(22) Xu, J.; Lin, F.; Nordlund, D.; Crumlin, E. J.; Wang, F.; Bai, J.; Doeff, M. M.; Tong, W. Elucidation of the surface characteristics and electrochemistry of high-performance $LiNiO_2$. *Chem. Commun.* **2016**, *52*, 4239−4242.
(23) Kim, J.; Lee, H.; Cha, H.; Yoon, M.; Park, M.; Cho, J. Prospect and Reality of Ni-Rich Cathode for Commercialization. *Adv. Energy Mater.* **2017**, *8*, 1702028.
(24) Olivetti, E. A.; Ceder, G.; Gaustad, G. G.; Fu, X. Lithium-Ion Battery Supply Chain Considerations: Analysis of Potential Bottlenecks in Critical Metals. *Joule* **2017**, *1*, 229−243.
(25) Chen, M. The Democratic Republic of Congo's other Crisis; The Nation. https://www.thenation.com/article/congo-china-mining-electronics/ (accessed Jan 25, 2019).
(26) Xie, Q.; Li, W.; Manthiram, A. A Mg-Doped High-Nickel Layered Oxide Cathode Enabling Safer, High-Energy-Density Li-Ion Batteries. *Chem. Mater.* **2019**, *31*, 938−946.
(27) Li, H.; Zhou, P.; Liu, F.; Li, H.; Cheng, F.; Chen, J. Stabilizing nickel-rich layered oxide cathodes by magnesium doping for rechargeable lithium-ion batteries. *Chem. Sci.* **2019**, *10*, 1374−1379.
(28) Kim, U.-H.; Jun, D.-W.; Park, K.-J.; Zhang, Q.; Kaghazchi, P.; Aurbach, D.; Major, D. T.; Goobes, G.; Dixit, M.; Leifer, N.; Wang, C. M.; Yan, P.; Ahn, D.; Kim, K.-H.; Yoon, C. S.; Sun, Y.-K. Pushing the limit of layered transition metal oxide cathodes for high-energy density rechargeable Li ion batteries. *Energy Environ. Sci.* **2018**, *11*, 1271−1279.
(29) Zhang, J.; Yang, Z.; Gao, R.; Gu, L.; Hu, Z.; Liu, X. Suppressing the Structure Deterioration of Ni-Rich $LiNi_{0.8}Co_{0.1}Mn_{0.1}O_2$ through Atom-Scale Interfacial Integration of Self-Forming Hierarchical Spinel Layer with Ni Gradient Concentration. *ACS Appl. Mater. Interfaces* **2017**, *9*, 29794−29803.
(30) Liu, Z.; Zhen, H.; Kim, Y.; Liang, C. Synthesis of $LiNiO_2$ cathode materials with homogeneous Al doping at the atomic level. *J. Power Sources* **2011**, *196*, 10201−10206.
(31) Ohzuku, T.; Ueda, A.; Kouguchi, M. Synthesis and Characterization of $LiAl_{1/4}Ni_{3/4}O_2$ ($R\bar{3}m$) for Lithium-Ion (Shuttlecock) Batteries. *J. Electrochem. Soc.* **1995**, *142*, 4033−4039.
(32) Croguennec, L.; Suard, E.; Willmann, P.; Delmas, C. Structural and Electrochemical Characterization of the $LiNi_{1-y}Ti_yO_2$ Electrode Materials Obtained by Direct Solid-State Reactions. *Chem. Mater.* **2002**, *14*, 2149−2157.
(33) Ha, H.-W.; Jeong, K. H.; Kim, K. Effect of titanium substitution in layered $LiNiO_2$ cathode material prepared by molten-salt synthesis. *J. Power Sources* **2006**, *161*, 606−611.
(34) Kim, J.; Amine, K. The effect of tetravalent titanium substitution in $LiNi_{1-x}Ti_xO_2$ ($0.025 \leq x \leq 0.2$) system. *Electrochem. Commun.* **2001**, *3*, 52−55.
(35) Sathiyamoorthi, R.; Shakkthivel, P.; Ramalakshmi, S.; Shul, Y.-G. Influence of Mg doping on the performance of $LiNiO_2$ matrix ceramic nanoparticles in high-voltage lithium-ion cells. *J. Power Sources* **2007**, *171*, 922−927.
(36) Muto, S.; Tatsumi, K.; Kojima, Y.; Oka, H.; Kondo, H.; Horibuchi, K.; Ukyo, Y. Effect of Mg-doping on the degradation of $LiNiO_2$-based cathode materials by combined spectroscopic methods. *J. Power Sources* **2012**, *205*, 449−455.
(37) Gao, Y.; Yakovleva, M. V.; Ebner, W. B. Novel $LiNi_{1-x}Ti_{x/2}Mg_{x/2}O_2$ Compounds as Cathode Materials for Safer Lithium-Ion Batteries. *Electrochem. Solid-State Lett.* **1999**, *1*, 117−119.
(38) Zhang, J.-N.; Li, Q.; Ouyang, C.; Yu, X.; Ge, M.; Huang, X.; Hu, E.; Ma, C.; Li, S.; Xiao, R.; Yang, W.; Chu, Y.; Liu, Y.; Yu, H.; Yang, X.-Q.; Huang, X.; Chen, L.; Li, H. Trace doping of multiple elements enables stable battery cycling of $LiCoO_2$ at 4.6 V. *Nat. Energy* **2019**, *4*, 594−603.
(39) Liu, Q.; Su, X.; Lei, D.; Qin, Y.; Wen, J.; Guo, F.; Wu, Y. A.; Rong, Y.; Kou, R.; Xiao, X.; Aguesse, F.; Bareño, J.; Ren, Y.; Lu, W.; Li, Y. Approaching the capacity limit of lithium cobalt oxide in lithium ion batteries via lanthanum and aluminium doping. *Nat. Energy* **2018**, *3*, 936−943.
(40) Wang, L.; Ma, J.; Wang, C.; Yu, X.; Liu, R.; Jiang, F.; Sun, X.; Du, A.; Zhou, X.; Cui, G. A Novel Bifunctional Self-Stabilized Strategy Enabling 4.6 V $LiCoO_2$ with Excellent Long-Term Cyclability and High-Rate Capability. *Adv. Sci.* **2019**, *6*, 1900355.
(41) Shin, Y.; Kan, W. H.; Aykol, M.; Papp, J. K.; McCloskey, B. D.; Chen, G.; Persson, K. A. Alleviating oxygen evolution from Li-excess oxide materials through theory-guided surface protection. *Nat. Commun.* **2018**, *9*, 4597.
(42) Pouillerie, C.; Croguennec, L.; Biensan, P.; Willmann, P.; Delmas, C. Synthesis and Characterization of New $LiNi_{1-y}Mg_yO_2$ Positive Electrode Materials for Lithium-Ion Batteries. *J. Electrochem. Soc.* **2000**, *147*, 2061−2069.

(43) Lopez, M. F.; Soriano, L.; Palomares, F. J.; Sanchez-Agudo, M.; Fuentes, G. G.; Gutiérrez, A.; Jiménez, J. A. Soft x-ray absorption spectroscopy study of oxide layers on titanium alloys. *Surf. Interface Anal.* **2002**, *33*, 570−576.
(44) Mu, L.; Lin, R.; Xu, R.; Han, L.; Xia, S.; Sokaras, D.; Steiner, J. D.; Weng, T.-C.; Nordlund, D.; Doeff, M. M.; Liu, Y.; Zhao, K.; Xin, H. L.; Lin, F. Oxygen Release Induced Chemomechanical Breakdown of Layered Cathode Materials. *Nano Lett.* **2018**, *18*, 3241−3249.
(45) Mu, L.; Feng, X.; Kou, R.; Zhang, Y.; Guo, H.; Tian, C.; Sun, C.-J.; Du, X.-W.; Nordlund, D.; Xin, H. L.; Lin, F. Deciphering the Cathode-Electrolyte Interfacial Chemistry in Sodium Layered Cathode Materials. *Adv. Energy Mater.* **2018**, *8*, 1801975.
(46) Yang, H.; Wu, H. H.; Ge, M.; Li, L.; Yuan, Y.; Yao, Q.; Chen, J.; Xia, L.; Zheng, J.; Chen, Z.; Duan, J.; Kisslinger, K.; Zeng, X. C.; Lee, W. K.; Zhang, Q.; Lu, J. Simultaneously Dual Modification of Ni-Rich Layered Oxide Cathode for High-Energy Lithium-Ion Batteries. *Adv. Funct. Mater.* **2019**, *29*, 1808825.
(47) Kim, Y. Effects and distribution of Zr introduced in Ni-based cathode material for Li-ion batteries. *Phys. Chem. Chem. Phys.* **2019**, *21*, 12505−12517.
(48) Steiner, J. D.; Cheng, H.; Walsh, J.; Zhang, Y.; Zydlewski, B.; Mu, L.; Xu, Z.; Rahman, M. M.; Sun, H.; Michel, F. M.; Sun, C.-J.; Nordlund, D.; Luo, W.; Zheng, J.-C.; Xin, H. L.; Lin, F. Targeted Surface Doping with Reversible Local Environment Improves Oxygen Stability at the Electrochemical Interfaces of Nickel-Rich Cathode Materials. *ACS Appl. Mater. Interfaces* **2019**, *11*, 37885.
(49) Jung, R.; Metzger, M.; Maglia, F.; Stinner, C.; Gasteiger, H. A. Oxygen Release and Its Effect on the Cycling Stability of $LiNi_xMn_yCo_zO_2$ (NMC) Cathode Materials for Li-Ion Batteries. *J. Electrochem. Soc.* **2017**, *164*, A1361−A1377.
(50) Beltrop, K.; Klein, S.; Nölle, R.; Wilken, A.; Lee, J. J.; Köster, T. K.-J.; Reiter, J.; Tao, L.; Liang, C.; Winter, M.; Qi, X.; Placke, T. Triphenylphosphine Oxide as Highly Effective Electrolyte Additive for Graphite/NMC811 Lithium Ion Cells. *Chem. Mater.* **2018**, *30*, 2726−2741.
(51) Arai, H.; Tsuda, M.; Sakurai, Y. Lithium nickelate electrodes with enhanced high-temperature performance and thermal stability. *J. Power Sources* **2000**, *90*, 76−81.
(52) Zhang, J.; Xue, L.; Li, Y.; Lei, T.; Deng, S.; Chen, Y.; Zhu, J.; Wang, S.; Guo, J. Suppressing Nickel Dissolution in Ni-rich Layered Oxide Cathodes Using NiF_2 as Electrolyte Additive. *ChemElectroChem* **2019**, *6*, 3125−3131.
(53) Jung, R.; Linsenmann, F.; Thomas, R.; Wandt, J.; Solchenbach, S.; Maglia, F.; Stinner, C.; Tromp, M.; Gasteiger, H. A. Nickel, Manganese, and Cobalt Dissolution from Ni-Rich NMC and Their Effects on NMC622-Graphite Cells. *J. Electrochem. Soc.* **2019**, *166*, A378−A389.
(54) MacNeil, D. D.; Lu, Z.; Chen, Z.; Dahn, J. R. A comparison of the electrode/electrolyte reaction at elevated temperatures for various Li-ion battery cathodes. *J. Power Sources* **2002**, *108*, 8−14.
(55) Kim, T.; Song, B.; Lunt, A. J. G.; Cibin, G.; Dent, A. J.; Lu, L.; Korsunsky, A. M. Operando X-ray Absorption Spectroscopy Study of Atomic Phase Reversibility with Wavelet Transform in the Lithium-Rich Manganese Based Oxide Cathode. *Chem. Mater.* **2016**, *28*, 4191−4203.
(56) Li, X.; Liu, J.; Banis, M. N.; Lushington, A.; Li, R.; Cai, M.; Sun, X. Atomic layer deposition of solid-state electrolyte coated cathode materials with superior high-voltage cycling behavior for lithium ion battery application. *Energy Environ. Sci.* **2014**, *7*, 768−778.
(57) Lee, Y.-S.; Ryu, K.-S. Study of the lithium diffusion properties and high rate performance of $TiNb_6O_{17}$ as an anode in lithium secondary battery. *Sci. Rep.* **2017**, *7*, 16617.
(58) Tian, J.; Su, Y.; Wu, F.; Xu, S.; Chen, F.; Chen, R.; Li, Q.; Li, J.; Sun, F.; Chen, S. High-Rate and Cycling-Stable Nickel-Rich Cathode Materials with Enhanced Li^+ Diffusion Pathway. *ACS Appl. Mater. Interfaces* **2016**, *8*, 582−587.
(59) Wei, Y.; Zheng, J.; Cui, S.; Song, X.; Su, Y.; Deng, W.; Wu, Z.; Wang, X.; Wang, W.; Rao, M.; Lin, Y.; Wang, C.; Amine, K.; Pan, F. Kinetics Tuning of Li-Ion Diffusion in Layered $Li(Ni_xMn_yCo_z)O_2$. *J. Am. Chem. Soc.* **2015**, *137*, 8364−8367.